

A single-cell transcriptome atlas reveals the trajectory of early cell fate transition during callus induction in *Arabidopsis*

Ruilian Yin^{1,2}, Ruiying Chen^{1,2}, Keke Xia^{2,*} and Xun Xu^{1,2,3,*}

¹College of Life Sciences, University of Chinese Academy of Sciences, Beijing 10049, China

²BGI Research, Beijing 102601, China

³Guangdong Provincial Key Laboratory of Genome Read and Write, BGI-Shenzhen, Shenzhen 518120, Guangdong, China

*Correspondence: Keke Xia (xiakeke@genomics.cn), Xun Xu (xuxun@genomics.cn)

<https://doi.org/10.1016/j.xplc.2024.100941>

ABSTRACT

The acquisition of pluripotent callus from somatic cells plays an important role in plant development studies and crop genetic improvement. This developmental process incorporates a series of cell fate transitions and reprogramming. However, our understanding of cell heterogeneity and mechanisms of cell fate transition during callus induction remains quite limited. Here, we report a time-series single-cell transcriptome experiment on *Arabidopsis* root explants that were induced in callus induction medium for 0, 1, and 4 days, and the construction of a detailed single-cell transcriptional atlas of the callus induction process. We identify the cell types responsible for initiating the early callus: lateral root primordium-initiating (LRPI)-like cells and quiescent center (QC)-like cells. LRPI-like cells are derived from xylem pole pericycle cells and are similar to lateral root primordia. We delineate the developmental trajectory of the dedifferentiation of LRPI-like cells into QC-like cells. QC-like cells are undifferentiated pluripotent acquired cells that appear in the early stages of callus formation and play a critical role in later callus development and organ regeneration. We also identify the transcription factors that regulate QC-like cells and the gene expression signatures that are related to cell fate decisions. Overall, our cell-lineage transcriptome atlas for callus induction provides a distinct perspective on cell fate transitions during callus formation, significantly improving our understanding of callus formation.

Key words: callus induction, single-cell RNA-seq, cell fate transition, developmental trajectory, transcriptional regulation, pluripotency

Yin R., Chen R., Xia K., and Xu X. (2024). A single-cell transcriptome atlas reveals the trajectory of early cell fate transition during callus induction in *Arabidopsis*. Plant Comm. 5, 100941.

INTRODUCTION

Under appropriate culture conditions, somatic plant cells retain the remarkable ability to regenerate organs or entire individuals. Tissue culture technology based on plant regeneration capacity is widely used for plant propagation, gene editing, and genetic improvement. In a typical tissue culture regeneration system, isolated explants are first cultured on a callus induction medium (CIM) to form a callus (a mixture of pluripotent cells), and the callus is then transferred to shoot induction medium (SIM) or root induction medium to regenerate new shoot or root tissues (Valvekens et al., 1988; Ikeuchi et al., 2013, 2019). During this process, callus formation from somatic cells is key for the acquisition of cell totipotency and necessary for the *de novo* regeneration of adventitious shoots or roots. However, for many crop species, callus induction represents a bottleneck that hinders genetic improvement studies (Ikeuchi et al.,

2019). Therefore, it is important to characterize the molecular mechanism(s) that underlie callus formation in plants.

Previously, researchers found that a CIM-induced callus develops in a similar manner to its original lateral roots, and it forms the tissue structure of a root meristem, characterized by the orderly division and differentiation of xylem pole pericycle (XPP) cells (Atta et al., 2009; Sugimoto et al., 2010; Fan et al., 2012). In the process of callus induction, XPP cells acquire cell identities that are similar to those of lateral root primordia or root meristems for the inducible expression of regulators of the development of both lateral roots and root meristems (Okushima et al., 2007; Fan et al., 2012; Liu

Published by the Plant Communications Shanghai Editorial Office in association with Cell Press, an imprint of Elsevier Inc., on behalf of CSPB and CEMPS, CAS.

et al., 2014; Chen et al., 2016; Hu and Xu, 2016). Culturing on CIM activates *AUXIN RESPONSE FACTOR 7 (ARF7)* and *ARF19*, which in turn promote the expression of *LATERAL ORGAN BOUNDARY DOMAIN 16 (LBD16)*, *LBD17*, *LBD18*, and *LBD29*. The expression of these *LBD* genes is necessary for callus formation (Okushima et al., 2007; Fan et al., 2012). Expression of *WUSCHEL-RELATED HOMEOBOX 11 (WOX11)* and *WOX12* is also activated and further prompts the reprogramming of regenerative cells into root founder cells. The activation of *WOX11/12* drives expression of the root stem cell regulatory genes *WOX5* and *WOX7*, which mediate induction of the niche pattern of the stem cell and activate the division of root founder cells into root primordium cells (Liu et al., 2014; Chen et al., 2016; Hu and Xu, 2016). Other regulatory factors of stem cells in the root meristem, such as *PLETHORA 3 (PLT3)*, *PLT5*, and *PLT7*, are also activated and promoted during the acquisition of callus pluripotency (Hofhuis et al., 2013; Kareem et al., 2015). Because callus formation involves a series of cell transitions, it remains to be clarified how the aforementioned regulatory factors are organized at the cellular level to ultimately specify the cell fate of a pluripotent callus.

The recent development of single-cell transcriptome sequencing (scRNA-seq) technology provides a unique opportunity to study regulators at cellular resolution (Shahan et al., 2021; Shaw et al., 2021; Mo and Jiao, 2022). Zhai and Xu (2021) reported the heterogeneity of a 6-day-old hypocotyl-derived callus. They found that the middle cell layer constituted potential pluripotent cells, similar to quiescent center (QC) cells, and could develop into vascular-like initial cells and epidermal-like cells. They also observed *WOX5/7* interacting with *PLT1/2* to facilitate *TAA1* expression, which determines the pluripotent status of the callus. In addition, Ogura et al. used scRNA-seq to generate a catalog of callus cells that underwent shoot apical meristem (SAM) formation on SIM for 7 days and found that the outer layer of cells contained SAM and non-meristematic cells. They also noted that the *WOX13-EXP/MAN7* pathway promoted cell expansion and differentiation, whereas the *WOX13-WUS* pathway negatively regulated SAM formation from the callus (Ogura et al., 2023). These single-cell studies highlight the great cell heterogeneity within the callus and the need to analyze the callus at the cellular level. To this end, it is crucial to study callus initiation. It is also important to study the mechanism of cell fate transition to better understand cell dedifferentiation, which remains poorly understood.

In this study, we performed time-series scRNA-seq to construct a single-cell transcriptome atlas of root-derived callus induction at an early stage. From this atlas, we successfully identified two important cell types, an LRPI-like cell and a QC-like cell, which are crucial transitional cell types that appear during callus induction. We also characterized the gene regulatory networks of the QC-like cells. These findings greatly enhance our understanding of cell fate transitions during callus induction.

RESULTS

Transcriptome atlas of callus induction at single-cell resolution

According to a previous study, a callus can be induced after explants are cultured on CIM for a few days (Sugimoto et al., 2010). We observed significant protrusions from the root explants after

Cell-lineage transcriptome atlas for callus induction

4 days of such induction (Supplemental Figure 1A), indicating that callus cells had already been induced by day 4 (CIM4). Thus, *Arabidopsis* root explants cultured on CIM for 0 (CIM0), 1 (CIM1), and 4 days were sampled to study the early stages of callus formation. Protoplasts were isolated and used for scRNA-seq (Figure 1A). After single-cell data processing, datasets for 25 188 single cells were obtained: 6184 cells for CIM0, 8777 cells for CIM1, and 10 227 cells for CIM4 (Supplemental Table 1). Because replications were performed at each time point, we first conducted a correlation analysis that showed that samples from the same time point clustered together and exhibited a high degree of similarity, confirming the reproducibility of these single-cell datasets (Supplemental Figure 1B). The datasets were then used for clustering; 26 cell clusters were obtained, and the cellular identities of most clusters were annotated.

Consistent with the actual identities of the explants, cells in CIM0 still maintained a root cell identity. Cell clusters 5, 10, 15, 16, 20, and 22 in CIM0 were annotated as stele, lateral root columella (LRC), columella, epidermis, XPP, and endodermis cells with enriched expression of root cell-type marker genes, such as the stele markers *ROOT MERISTEM GROWTH FACTOR 8 (RGF8)* (Fernandez et al., 2020) and *HISTONE ACETYLTRANSFERASE 1 (HAG1)* (Kim et al., 2018), the LRC marker *AT1G66800* (Efroni et al., 2016), the columella marker *ALPHA-GLUCAN PHOSPHORYLASE 2 (PHS2)* (Ryu et al., 2019), the epidermis marker *ANTHOCYANINLESS2 (ANL2)* (Efroni et al., 2016), the XPP marker gene *XYLOGLUCAN ENDOTRANSGLUCOSYLASE/HYDROLASE 21 (XTH21)* (Jean-Baptiste et al., 2019), and the endodermis marker *GASA7 (AT2G14900)* (Serrano-Ron et al., 2021) (Figure 1B; Supplemental Figure 2B). Cluster 3 of CIM0 was enriched in marker genes related to the root apical meristem, such as *RGF3* (Matsuzaki et al., 2010) and *PLT1* (Aida et al., 2004) (Supplemental Figure 2B and 2E), as well as the wounding-related genes *WIND1/2* (Ikeuchi et al., 2017) and genes associated with jasmonic acid (JA) signaling and synthesis (Supplemental Figure 2C). This is consistent with the explants having been cut during the process of explant preparation. These characteristics suggest that cluster 3 represents the initial group of cells that respond to wounding stress and activate root meristem activity. Cells in cluster 3 were annotated as response cell types (Figure 1B). After this, cells with stem-cell and pluripotent activity appeared with callus induction (Figure 1B–1D). Clusters 4 and 7 were the main cell types of CIM1; they were annotated as vascular-like cells with stem cell activity, and they specifically expressed the stem cell regulator *BABY BOOM (BBM)* and the plant peptide growth factor *PSK5* (Ikeuchi et al., 2019) (Figure 1B and 1C; Supplemental Figure 2B). We also found potential pluripotent cells mainly at CIM4, clusters 9 and 19. These showed enriched expression of the QC markers *WOX5* (Zhang et al., 2015; Hu and Xu, 2016) and *PI* in cluster 9 (Figure 1C) and the regeneration-related markers *ESR1* (Iwase et al., 2017), *PATATIN-like protein 6 (PLP6)* (Efroni et al., 2016), *FAD-binding Berberine enzyme (FAD-BD)* (Xu et al., 2018), *PHABULOSA (PHB)* (Zhang et al., 2017), and *PHAVOLUTA (PHV)* (Ikeuchi et al., 2019) in cluster 19 (Figure 1C; Supplemental Figure 2B). Taking into account that callus initiation is similar to lateral root initiation (Atta et al., 2009; Sugimoto et al., 2010) and that lateral root primordium initiation (LRPI) genes were significantly enriched in cluster 9 (Supplemental Figure 2F), we annotated cluster 9 as LRPI-like cells. In addition, we evaluated

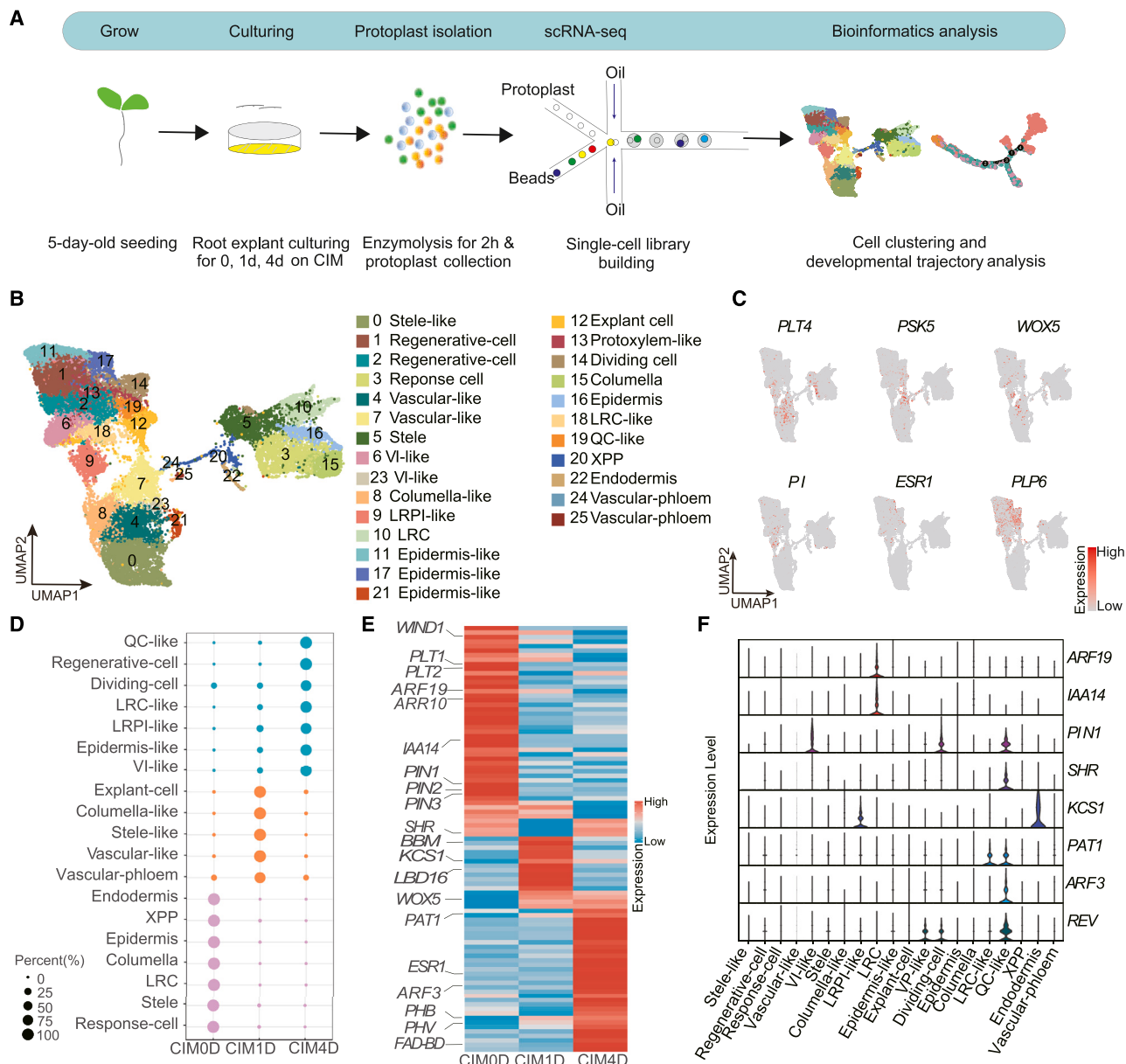


Figure 1. Transcriptional profiling of early callus initiation at single-cell resolution.

(A) Experimental design: *Arabidopsis thaliana* seedlings were grown for 5 days on 1/2 MS medium, and the root portion was then taken and cultured on CIM for 0, 1, and 4 days. Protoplasts were prepared from root explants for single-cell RNA-seq.

(B) Visualization of all cells of CIM0/1/4 with UMAP, organized into 26 clusters. Dots represent individual cells, and colors indicate cell clusters. See also *Supplemental Figure 2B*. The dot plot of marker genes shows the cell identities of each cell cluster. Average expression indicates normalized and scaled unique molecular identifiers (UMIs).

(C) UMAP plot showing selected marker genes for vascular-like, LRPI-like, and QC-like cells. The full names and referenced expression patterns of selected genes are summarized in *Supplemental Table 2*.

(D) Dot plot showing cell types and proportions in CIM0, CIM1, and CIM4.

(E) Heatmap showing changes in the expression of genes associated with callus formation and regeneration based on scRNA-seq data.

(F) Violin plot showing the expression patterns of genes involved in callus formation in specific cell types.

the expression of pluripotency genes to assess the pluripotency of cell clusters. We observed that cluster 19 had the highest pluripotency score, indicating that it represents a population of highly plastic pluripotent cells (*Supplemental Figure 2G*). Thus, we annotated cluster 19 as QC-like cells. Overall, our annotations provided a panoramic picture of the cell population in the early stages of callus formation.

Previous studies have identified many regulators involved in callus formation (*Ikeuchi et al., 2013, 2019*). In our dataset, we found that the wound-responsive genes *WIND1/2/3* and the auxin transporter regulatory genes *PIN-FORMED 1 (PIN1)* and *PIN2/3* were specifically enriched in CIM0. *BBM*, *ARF5*, *LBD16*, *WOX5*, *KCS1*, and other genes that regulate stem-cell characteristics and early embryo fate were specifically enriched in CIM1

(Figure 1E). *WOX5*, *PLT5/7*, *SHR*, *REV*, and other genes that regulate meristem characteristics and auxin were enriched in CIM4 (Figure 1E). We also found that CIM1 genes, such as *KCS1*, were particularly expressed in LRPI-like cells, whereas CIM4 genes such as *SHR* and *REV* were mainly expressed in QC-like cells (Figure 1E and 1F). These results reflect the importance of LRPI-like cells and QC-like cells in callus formation.

Thus far, we have constructed a single-cell transcriptome atlas that reveals substantial cell heterogeneity and rapid cell fate transition profiles during callus formation. This atlas will help to facilitate the exploration of functional cell types and regulators.

LRPI-like cells represent a transitional cell type during callus induction

Because callus formed in response to CIM induction shares an initial developmental program with lateral root formation (Sugimoto et al., 2010), we were able to identify a new cell type related to lateral root initiation, the LRPI-like cells. Next, we performed pseudo-time analysis using Monocle 3 to construct cell developmental trajectories showing how these root identity cells gradually develop into pluripotent callus cells and the involvement of LRPI-like cells, which are still largely unknown. In general, we observed that the cell types of CIM0 and CIM4 were set separately as the initial and terminal stages of the developmental process, and the cell types of CIM1 were found at the intermediate stage (Figure 2A). This was consistent with the time series of explants. At the cell-type level, we observed that XPP was the initial cell type and served as a connecting point between CIM0 and CIM1 cells (Figure 2B). These results are consistent with previous reports that XPP cells are the precursors of callus cells, which has been confirmed at the molecular level (Atta et al., 2009; Sugimoto et al., 2010; Eshed Williams, 2021). Zhu et al. (2023) revealed that primary vascular cells are the main initiating cell type for cotton callus. We compared these two datasets and found that genes that were specifically expressed in cotton primary vascular cells were also enriched in *Arabidopsis* CIM1 cells, and the largest proportion of genes were co-expressed with *Arabidopsis* XPP cells and vascular phloem (Supplemental Figure 3). These similar regulators in *Arabidopsis* and cotton indicate a common mechanism of callus induction in the two species. Along the trajectories, we observed that LRPI-like cells followed two other cell types, vascular-initiation-like (VI-like) cells and columella-like cells (Figure 2B), showing that LRPI-like cells participated in callus formation and acted as an intermediate cellular state during callus formation. We also observed that LRPI-like cells formed a connecting node between CIM1 and CIM4 cells, with potential to develop into other cell types of CIM4. The developmental trajectories diverged and separated into two developmental directions for CIM4 cells, showing that LRPI-like cells had the potential to develop into epidermis-like and QC-like cells (Figure 2A and 2B). The connecting node and divergence of cell fate identities of LRPI-like cells indicate that these cells have a vital transitional role during callus induction.

To further explore the roles of LRPI-like cells, we analyzed the patterns of gene expression along the developmental trajectories. In all, 17 gene modules were revealed, and module 17

was specifically enriched in LRPI-like cells (Figure 2C and 2D). Next, we extracted the genes of that module (Supplemental Table 3) and performed Gene Ontology (GO) enrichment analysis. Among the top 20 enriched GO terms were cuticle development, lipid transport, fatty acid derivative metabolic process, wax biosynthetic process, and very-long-chain fatty acid (VLCFA) metabolic process (Figure 2E). Previous studies have reported that certain lipid molecules may participate in the transmission of cell signals to regulate cell proliferation and differentiation (DeBono et al., 2009; Lu et al., 2021). We observed that two genes encoding members of the 3-ketoacyl-CoA synthase family, *KCS6* and *KCS10*, were significantly expressed in LRPI-like cells and that genes encoding the lipid transporters *LTP1* and *LTP2* were also highly enriched in LRPI-like cells (Figure 2F). These results provide further evidence that LRPI-like cells play specific roles in regulating fatty acid biosynthetic and transport processes. Together, our findings suggest that the newly identified LRPI-like cells act as crucial transitional cell types and are involved in the mediation of callus induction, mainly by regulating fatty acid biosynthetic and transport processes.

LRPI-like cells can develop into QC-like cells with greater pluripotent identity

Because LRPI-like cells have two developmental directions, one of which is toward developing into QC-like cells that exhibit the greatest pluripotency (Figure 2A), there is great value in understanding this trajectory to better understand callus induction. We therefore performed additional analyses to confirm this developmental relationship. First, we isolated CIM4 callus cells, including LRPI-like cells, VI-like cells, vascular-protoxylem-like cells, epidermis-like cells, QC-like cells, and regenerative cells. We used CytoTRACE, a tool that can predict the relative differentiation status of cells by detecting reductions in transcriptional diversity as markers of pseudo-frequency projections along trajectories to estimate the cells' capacity to differentiate (Gulati et al., 2020). The results showed that QC-like cells were ordered first, epidermis-like cells were last, and LRPI-like cells were located between these two cell types (Figure 3A–3C). These results are consistent with previous trajectory analyses in which QC-like cells were the least differentiated and were derived from the moderately differentiated LRPI-like cells during dedifferentiation (Figure 2A–2C).

We also performed Monocle 2 analysis (Figure 3D) to verify the developmental trajectories of LRPI-like cells into QC-like cells. We separated regenerative cells (cluster 2), VI-like cells (cluster 6), QC-like cells (cluster 9), and LRPI-like cells (cluster 19) and reconstructed their developmental trajectories using Monocle 2 after visualizing the trajectory with DDRTree (Figure 3D). Consistent with the developmental trajectory shown in Figure 2A, LRPI-like cells were mainly distributed across the early stage of the pseudo-time trajectory, QC-like cells were mainly distributed in the late stages, and the other two cell types were largely distributed in the middle stage (Figure 3D; Supplemental Figure 4A). We also noted that the LRPI-like cell type contained two samples, CIM1 and CIM4, and we detected a number of genes downregulated in CIM4 (Supplemental Figure 4B). The change in gene expression

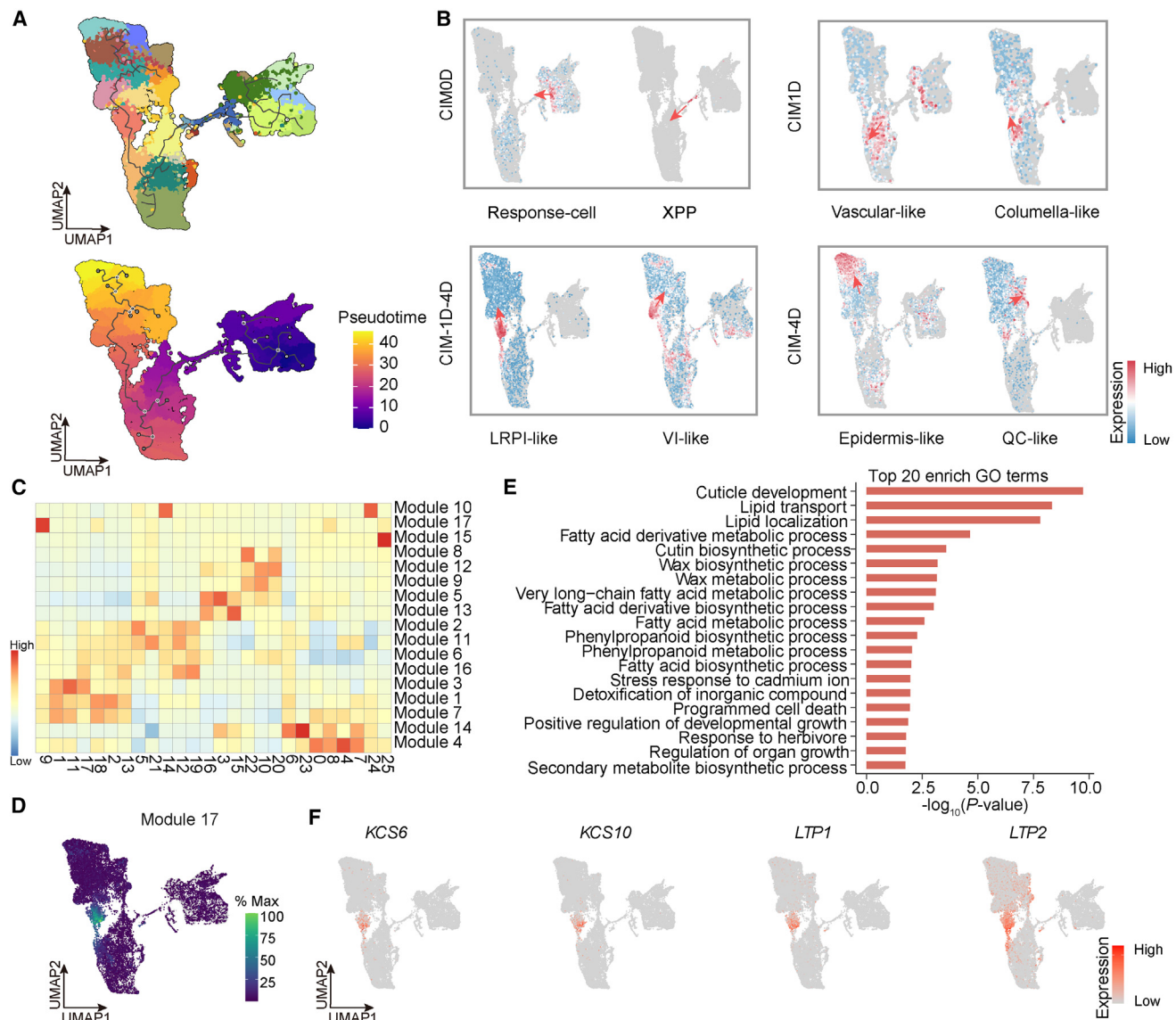


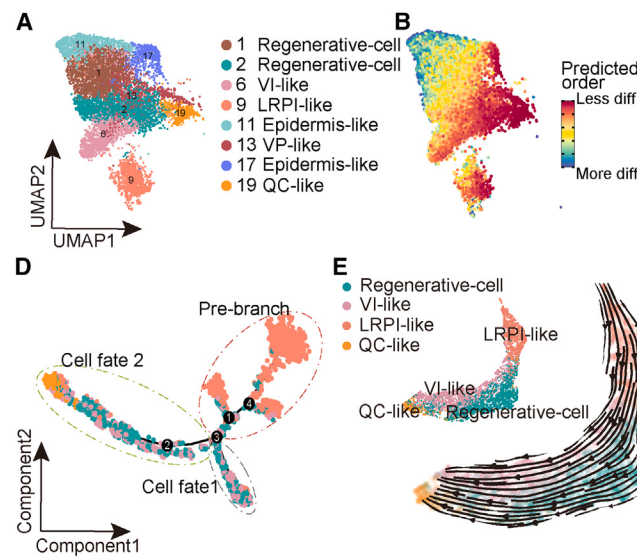
Figure 2. LRPI-like cells are a transitional cell type during callus initiation.

- (A) Monocle 3 analysis showing the callus developmental trajectory from CIM0 to CIM4, colored by Seurat clusters (top) and pseudo-time (bottom). Dark line: predicted pseudo-time trajectories. White dots: root nodes.
- (B) UMAP plot showing developmental changes in cell types over pseudo-time trajectories. The red arrows indicate the direction of development. The cell-type-specific enriched genes in Figure 2B are *PLT1* (response cell), *XTH21* (XPP), *BBM* (vascular-like cell), *NCED2* (columella-like), *LTP3* (LRPI-like), *HSP23.6* (VI-like), *AT4G39836* (epidermis-like), and *FAD-BD* (QC-like), and these genes are specifically expressed in the corresponding cell types. Detailed information on these genes is given in [Supplemental Table 2](#).
- (C) There are 17 modules in total for the specific enrichment patterns of genes that change along pseudo-time trajectories. Genes specifically enriched in LRPI-like cells (cluster 9) are module 17. The numbers at the bottom of the figure represent cell clusters, and the numbers on the right side of the figure represent the 17 modules.
- (D) UMAP plot showing genes in module 17 that are specifically enriched in LRPI-like cells.
- (E) Top 20 enriched GO terms for the genes in module 17.
- (F) UMAP plot showing selected representative genes in module 17.

indicates that LRPI-like cells indeed undergo dramatic transcriptomic changes and preparation for their late cell-fate transition. As shown in Figure 3D, the developmental trajectory of LRPI-like cells was divided into two branches (Figure 3D). The branch containing VI-like cells and regenerative cells was designated cell fate 1. Another branch that predominantly contained a high proportion of QC-like cells at the end of the

trajectory was designated cell fate 2 (Figure 3D; [Supplemental Figure 4A](#)). We also observed that the expression of genes known to regulate callus formation and shoot regeneration gradually increased and was significantly enriched at the endpoint; these included *ARF5* ([Efroni et al., 2016](#)), *XTH19/20* ([Pitaksaringkarn et al., 2014](#)), *FAD-BD* ([Xu et al., 2018](#)), *PHB* ([Zhang et al., 2017](#)), and *METHYLTRANSFERASE 1* (*MET1*)

Plant Communications



Cell-lineage transcriptome atlas for callus induction

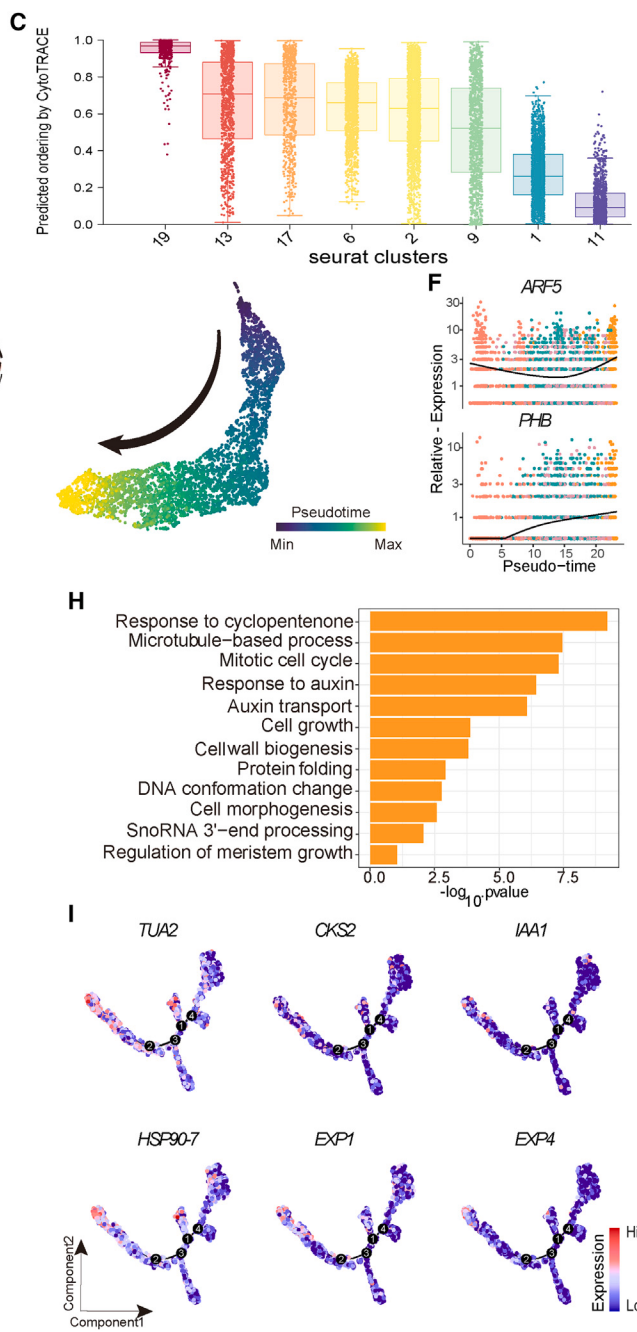


Figure 3. LRPI-like cells may develop into QC-like cells with greater pluripotency.

(A) UMAP plot showing the cell population extracted from CIM4.

(B) UMAP plot showing the cell differentiation ability predicted by CytoTrace. Blue indicates more differentiated cells, and dark red indicates less differentiated cells.

(C) Cell differentiation ability score predicted by CytoTrace; the degree of cell differentiation gradually increases from left to right.

(D) Distribution of LRPI-like cells (cluster 9), regenerative cells (cluster 2), and VI-like cells (cluster 6) on the pseudo-time trajectory branches, including pre-branch, cell fate 1, and cell fate 2.

(E) Cell developmental trajectories inferred using scTour. The arrow represents the future developmental direction of the cell.

(F) Expression of typical marker genes along pseudo-time. The black line indicates the expression tendency. Dots are individual cells.

(G) Heatmap displaying changes in gene expression along the pseudo-time trajectory branches. These genes were clustered into four modules with distinct expression patterns. Different colors represent the level of gene expression.

(H) Representative Gene Ontology (GO) terms in module 3.

(I) Expression pattern of genes associated with the auxin signaling pathway, cell division, and the response to cyclopentenone along pseudo-time.

(Liu et al., 2018a) (Figure 3F; Supplemental Figure 4C). Next, we used scTour, which can predict the underlying dynamics of unseen cellular states or new independent datasets with precision (Li, 2023), to verify the reconstructed developmental trajectories. One trajectory predicted by scTour showed that LRPI-like cells develop toward VI-like and regenerative cells, ending with QC-like cells, consistent with the results of Monocle 2 (Figure 3E). Furthermore, removal of LRPI-like cells from CIM4 produced a developmental gap between LRPI-like cells and VI-like ones; nevertheless, there was still a trend of development from LRPI-like cells at the initiation point to QC-like cells at the endpoint (Supplemental Figure 4D). Taken together, these results regarding cell differentiation status and cell developmental trajectories indicate that LRPI-like cells dedifferentiate into QC-like cells, with a higher pluripotent identity.

We next analyzed gene expression patterns along the later stages of the reconstructed developmental trajectories and explored four gene expression modules (Figure 3G). Genes enriched in module 3 were gradually highly expressed at the end of cell fate 2 (Figure 3G), and these genes may play an important role in regulating the development of QC-like cells. Next, we examined the functions of genes in module 3. As expected, genes in this module were associated with many GO terms related to the mitotic cell cycle, response to auxin, auxin transport, and cell growth (Figure 3E and 3F). Representative genes involved in auxin response and cell division, including *TUBULIN ALPHA-2* (*TUA2*), *CDK-SUBUNIT 2* (*CKS2*), and *IAA1*, showed increased expression from clusters 2 and 6 (regenerative and VI-like cells, respectively) to cluster 19 (QC-like cells) (Figure 3H and 3I). These results indicate that QC-like cells have rich auxin distribution and transport activities that enable them to promote cell growth and expansion. The enriched GO terms for genes in module 3 were consistently related to the regulation of meristem growth. The representative gene *HEAT SHOCK PROTEIN 90-7* (*HSP90-7*) (Ishiguro et al., 2002), which is involved in regulation of the meristem, was significantly enriched in QC-like cells at the endpoint of cell fate 2 (Figure 3I), indicating a higher percentage of pluripotent cells in the late stage of the pseudo-time axis. *EXPANSIN 1* (*EXPA1*) and *EXPA4* also gradually increased in expression together with the development of cell fate 2 (Figure 3I), and GO analysis indicated that their functions include cell wall biosynthesis (Figure 3H). This is consistent with the cell wall remodeling activity that takes place during callus formation (Ikeuchi et al., 2013). In addition, certain specific GO terms were enriched in module 3, including “response to cyclopentenone,” “DNA conformation change,” and “snoRNA 3' end processing” (Figure 3H). These biological processes involve the regulation of chromatin structure and accessibility, ribosome modification, and protein synthesis (Barneche et al., 2000; Stintzi et al., 2001; Albini et al., 2019). This demonstrates that QC-like cells play an extremely active role in transcription, and they produce more abundant transcripts to meet the high demand for new cell-wall and membrane components. Taken together, our results suggest that QC-like cells that develop from LRPI-like cells are in a weakly differentiated state and exhibit enhanced pluripotency and a range of transcriptional activities that regulate callus development, indicating the potential for unique roles in subsequent callus development.

QC-like cells are specialized for callus induction but not lateral root development

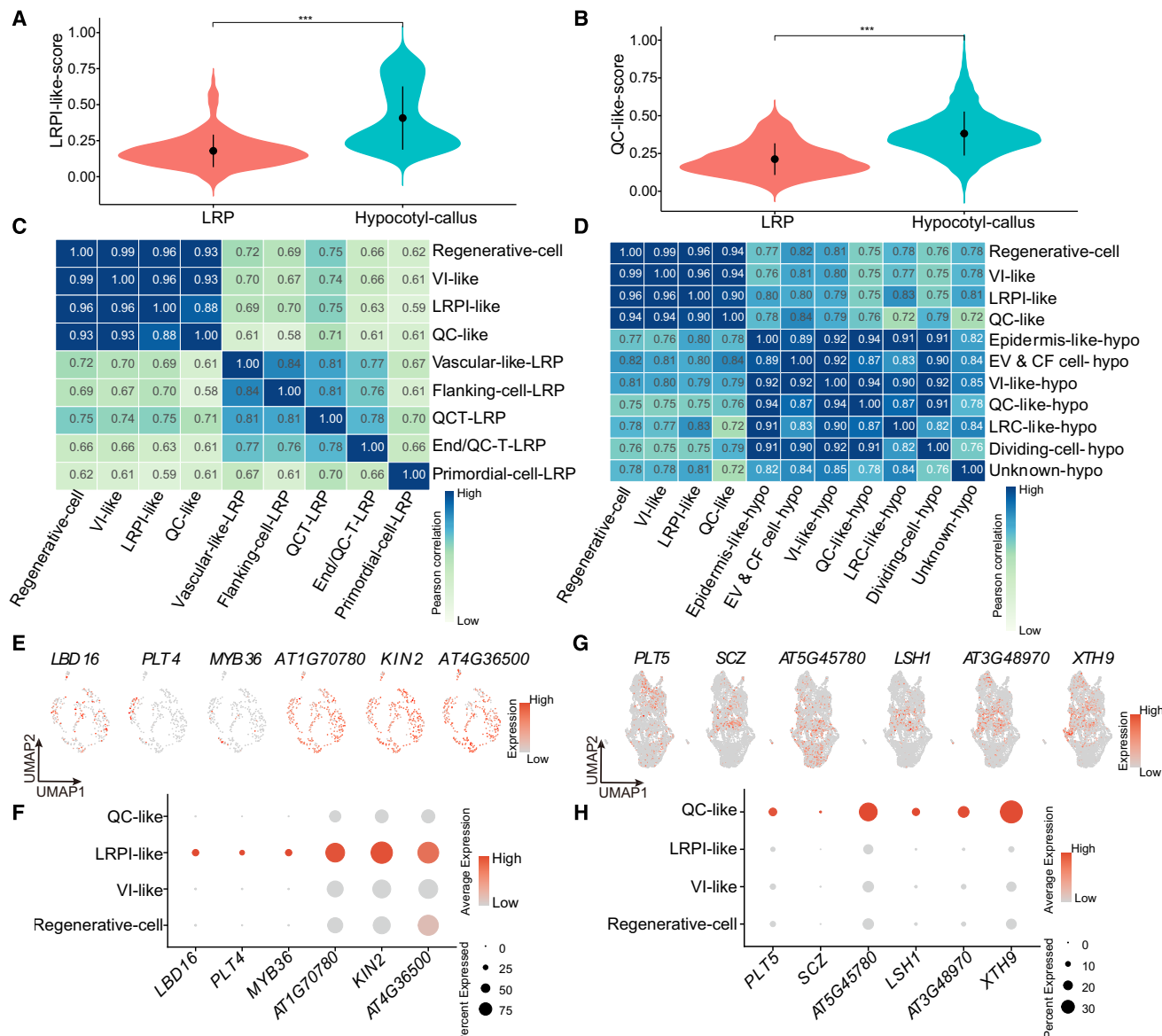
Previous studies have shown that callus consists of a tissue structure similar to that of LRP (Sugimoto et al., 2010; Fan et al., 2012). Here, we identified a new cell type, the LRPI-like cells, which exhibit specific LRP identities and may ultimately develop into callus cells. It would be valuable to understand what determines cell development into a callus rather than a lateral root.

First, we evaluated the expression scores of genes highly expressed in LRPI-like and QC-like cells in LRP cells at 4 days (Serrano-Ron et al., 2021) and hypocotyl-derived callus cells incubated in CIM for 6 days (Zhai and Xu, 2021) (Figure 4A and 4B). The results showed that DEGs for the two cell types had higher scores in hypocotyl-derived callus cells, and the DEG expression scores for the LRPI-like cells were relatively higher in LRP cells (Figure 4A and 4B). These results are consistent with those of callus induction culturing and indicate that there are significant differences in gene expression and cell identity between callus formation and lateral root development that likely play an important role in determining the direction of these cells' development into callus cells.

To explore the cell identities of LRPI-like and QC-like cells, we compared them with the cell subtypes of previously reported LRP cells and hypocotyl callus cells. First, we divided LRP cells and hypocotyl callus cells into subpopulations, assigning them cell labels (Supplemental Figure 5A–5D). Using a previously described method (Serrano-Ron et al., 2021), we divided 282 LRP cells into six subgroups and annotated them into five main cell types, including vascular-like cells, QC-transition cells (QCTs), endodermis/QC transition cells (End/QC-Ts), flanking cells, and primordial cells (Supplemental Figure 5A and 5B). Similarly, hypocotyl callus cells were divided into seven subgroups and annotated into six main cell types, including epidermis-like, explant vascular and callus founder (EV & CF), VI-like, QC-like, LRC-like, and dividing cells (Supplemental Figure 5C and 5D).

Next, we analyzed the correlations among the callus cell types involved in the reconstructed QC-like cell dedifferentiation trajectory shown in Figure 3C and LRP cells and hypocotyl-derived callus cells (Figure 4C and 4D). At the early stage of the dedifferentiation trajectory, LRPI-like cells had the highest correlation with QCT-LRP cells, whereas QC-like cells located at the end of the dedifferentiation trajectory had the lowest correlation with these cells (Figure 4C). Instead, with respect to hypocotyl-derived callus cells, QC-like cells had a significant correlation with EV & CF cells (-hypo) and QC-like cells (-hypo) (Figure 4D). These results indicate that there are significant differences in cell identity between LPRI-like cells and QC-like cells while also showing the novelty of the discovery of these two cell types in *Arabidopsis*.

We also searched for co-expressed genes between cell types exhibiting extremely significant correlations to validate the cell identities illustrated above. Genes known to participate in regulating lateral root formation and development, such as *LBD16* (Okushima et al., 2007), *PLT4* (Serrano-Ron et al., 2021), *MYB*

**Figure 4.** QC-like cells play a specific role in callus initiation but not lateral root development.

- (A) Expression scores for DEGs of LRPI-like cells in single-cell datasets obtained from LRP and hypocotyl callus.
- (B) Expression scores for DEGs of QC-like cells in single-cell datasets obtained from LRP and hypocotyl callus.
- (C) Heatmap showing correlations between the cells in the pseudo-time trajectory in Figure 2D and the cell subtypes of LRP.
- (D) Heatmap showing correlations between the cells in the pseudo-time trajectory in Figure 2D and the cell subtypes of hypocotyl callus.
- (E) UMAP plot showing selected representative genes in LRP cells.
- (F) Genes specifically expressed in LRP cells that were also specifically expressed in LRPI-like cells. The four cell types represent cells distributed along the pseudo-time trajectory in Figure 2D.
- (G) UMAP plot showing selected representative genes in hypocotyl callus cells.
- (H) Genes specifically expressed in hypocotyl callus cells that were also specifically expressed in LRPI-like cells. The four cell types represent the cells distributed along the pseudo-time trajectory in Figure 2D.

DOMAIN PROTEIN 36 (MYB36) (Serrano-Ron et al., 2021), and some potential regulatory genes, such as AT1G70780, STRESS-RESPONSIVE PROTEIN (KIN2), and AT4G36500, were highly expressed in LRP cells (Figure 4E). Along the developmental trajectories of QC-like cells, these lateral root identity genes were highly expressed in LRPI-like cells, and this expression was significantly inhibited and undetectable in QC-like cells from CIM4 callus (Figure 4F). It is interesting that

callus identity genes were significantly induced, particularly in QC-like cells. For example, genes involved in regulating the acquisition of pluripotency in callus cells, such as the stem cell regulatory factors PLT5 (Ikeuchi et al., 2017) and SCHIZORIZA (SCZ) (Pernas et al., 2010), were highly expressed in EV & CF cells and in QC-like cells in CIM6 hypocotyl callus (Figure 4G). They were also significantly enriched in QC-like cells of the CIM4 callus (Figure 4H).

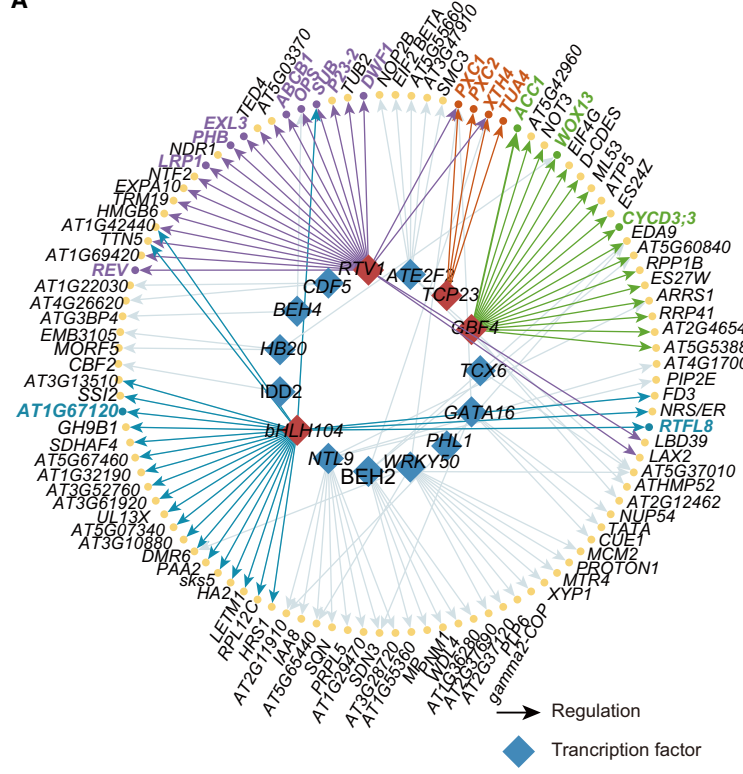
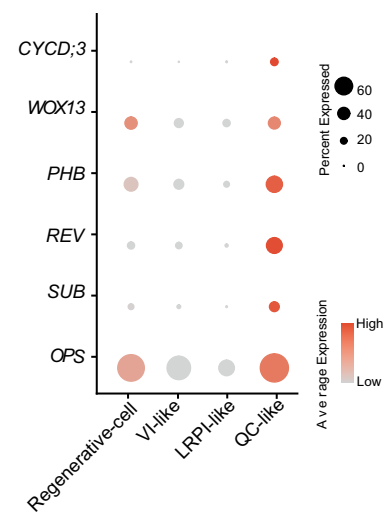
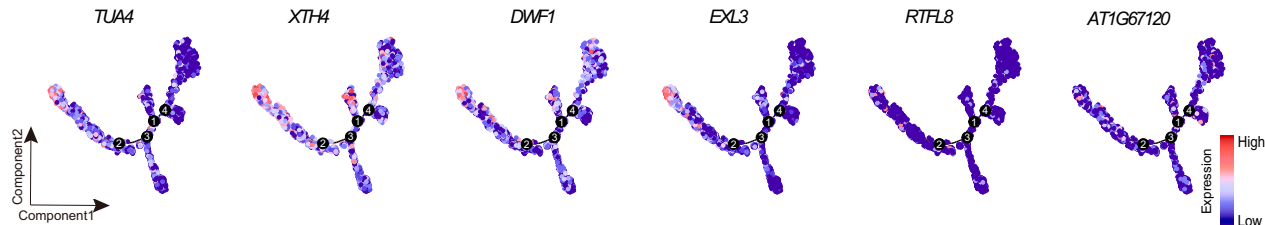
A**B****C**

Figure 5. Activation of a unique TF-regulatory network (TFRN) underlies regenerative competence of QC-like cells.

(A) The regulatory network consists of 16 transcription factors and 106 target genes. Squares represent transcription factors, circles represent target genes, and arrows represent regulation.

(B) Expression patterns of target genes related to the regulation of callus formation in TFRNs in all callus cells.

(C) Expression patterns of module 3 genes regulated by *TCP23*, *RTV1*, and *bHLH104* in the dedifferentiation trajectory.

These results demonstrate that lateral root identities gradually weakened, while pluripotent identities were gradually induced and enriched in QC-like cells during the cell-fate transition from LRPI-like cells to QC-like cells. The process of development into QC-like cells is likely to be specific for callus formation and should facilitate the formation of callus rather than lateral roots.

Activation of a unique transcription factor regulatory network underlies regenerative competence in QC-like cells

Because QC-like cells appear to be a crucial cell type specific for callus development, we explored the key regulators involved in the formation of these cells. We conducted a transcription factor regulatory network (TFRN) analysis using pySCENIC (Cao et al., 2023). From the analysis of all gene expression data in QC-like cells, we identified 16 new TFs and 106 potentially regulated target genes. From these findings, we con-

structed a TFRN of QC-like cells (Figure 5A). In this TFRN, we identified some genes that are known to be involved in the regulation of callus formation and shoot regeneration, such as *WOX13*, a member of the *WOX* family that promotes tissue repair (Ikeuchi et al., 2022); *CYCLIN D3;3* (*CYCD3;3*), which regulates cell population proliferation (Forzani et al., 2014); and the class III homeodomain-leucine zipper (HD ZIP III) TFs *PHABULOSA* (*PHB*) and *REVOLUTA* (*REV*), which play a key regulatory role in shoot regeneration (Zhang et al., 2017; Ikeuchi et al., 2019) (Figure 5A). These target genes are specifically enriched in QC-like cells along the developmental trajectories of LRPI-like cells into QC-like cells (Figure 5B). Furthermore, we found that *TCP DOMAIN PROTEIN 23* (*TCP23*), *G-BOX BINDING FACTOR 4* (*GBF4*), and *VERNALIZATION1* (*RTV1*) were responsible for the regulation of these genes, indicating that these three regulatory factors and their target genes may be involved in regulating the development of QC-like cells.

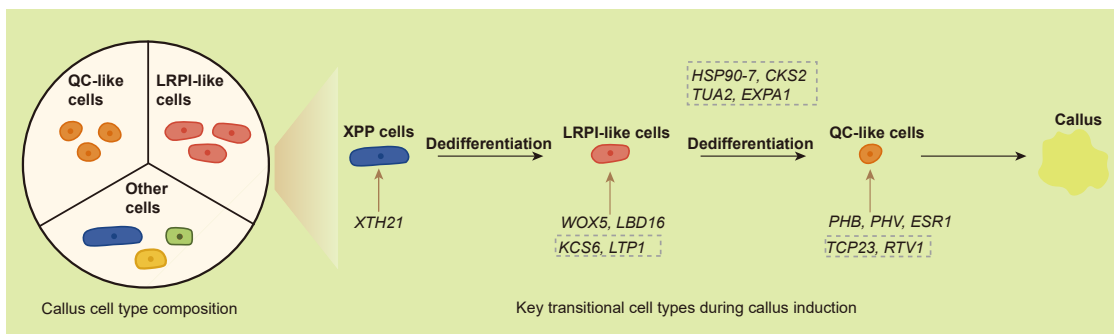


Figure 6. A model of the early cell fate transition during callus induction.

The cellular composition of a callus, the key cell types of the dedifferentiation process, and potential regulatory factors are essential for a comprehensive understanding of callus formation. During the key cell-fate transition process, XPP cells dedifferentiate into LRPI-like cells, which further transition into QC-like cells. Subsequently, QC-like cells develop into pluripotent cells within the callus tissue. *XTH21* is a marker gene for XPP cells; *WOX5* and *LBD16* are marker genes for LRPI-like cells; *KCS6* and *LTP1* in the dashed boxes are potential regulatory genes for LRPI-like cells; *PHB*, *PHV*, and *ESR1* are marker genes for QC-like cells; *TCP23* and *RTV1* in the dashed boxes are potential regulatory genes for QC-like cells. *HSP90-7*, *CKS2*, *TUA2*, and *EXP41* in the dashed boxes are potential regulatory genes involved in regulating the dedifferentiation of LRPI-like cells into QC-like cells. The circles represent different cell types, with colors denoting their identities. Genes in dashed boxes are potential regulators.

We previously analyzed the importance of genes in module 3 that significantly increased in expression during the formation of QC-like cells, as shown in Figure 3F and 3G. Next, we explored the genes that were potentially most responsible for callus formation and performed intersection analysis of them in module 3 and TFRN. We found 20 such genes (Figure 5A; Supplemental Table 5). GO analysis indicated that their functions mainly included cell wall biosynthesis, microtubule-based processes, and meristem development (Figure 3G and 3H). For example, *TUBULIN ALPHA-4* (*TUA4*) is involved in microtubule regulation, *ENDOXYLOGLUCAN TRANSFERASE* (*XTH4*) and *DWARF 1* (*DWF1*) are involved in auxin response and cell wall biosynthesis, and *EXORDIUM-like 3* (*EXL3*), *ROTUNDIFOLIA-like 8* (*RTFL8*), and *AT1G67120* are involved in the regulation of meristem development and cell proliferation. All of these genes are enriched in QC-like cells at a late stage of the pseudo-time trajectory (Figure 5C). According to the constructed TFRN, *TCP23*, *RTV1*, and *bHLH104* were the main upstream regulators of these target genes in module 3, which implies that these genes may play an important role in regulating the development of QC-like cells. Further functional analysis of these genes may shed light on how cell fate transition is determined.

In conclusion, we constructed a single-cell transcriptome atlas of the early stage of callus formation, and we identified LRPI-like cells and QC-like cells as key transitional cell types that facilitate callus formation (Figure 6). The gene regulators identified here also represent a valuable resource for further research.

DISCUSSION

Over the past few decades, various genes and gene regulatory pathways involved in regulating callus development have been identified (Ikeuchi et al., 2013, 2019; Hu and Xu, 2016; Liu et al., 2018b). However, because we have had limited information on cell heterogeneity during callus formation, it has been unclear how these genes are differently organized in various cell types, which in turn determines cell fate and promotes the formation of pluripotent callus cells. These limitations also hinder the wide

application of plant cell totipotency in plant studies and agriculture. Zhai and Xu performed scRNA-seq of hypocotyl-derived callus and showed that pluripotent callus originated in the middle layer of the callus (Zhai and Xu, 2021). However, only callus cultured on CIM for 6 days was sampled for single-cell RNA-seq, and so the question of how pluripotent callus cells were gradually induced could not be addressed. In the present study, explants induced on CIM for 0, 1, and 4 days were sampled for single-cell RNA-seq, and we generated a time-series single-cell transcriptome atlas of callus formation that revealed multiple cell types, including vascular-like, epidermal-like, LRPI-like, and QC-like cells. This atlas greatly improves our understanding of cell heterogeneity in callus formation.

We successfully investigated early cell fate transitions and the acquisition of regenerative competence during callus formation. We also identified two new types of pluripotent callus cell populations. The first was LRPI-like cells, which retain the characteristics of the original stem cells, and the other was the newly emerging QC-like cells. In general, we constructed a developmental trajectory in which XPP cells develop into LRPI-like cells and then into QC-like cells (Figure 6). Together with these developmental trajectories, the predicted result that XPP acts as an initiating cell type is supported by previous studies (Atta et al., 2009; Sugimoto et al., 2010; Eshed Williams, 2021). In addition, the XPP cells subsequently develop into LRPI-like cells with lateral root identities, which is also consistent with previous findings that callus formation shares the initial program of lateral root development. These findings provide additional evidence to confirm the reliability of the reconstructed developmental trajectories through the early stages of callus induction.

Along the developmental trajectories that we constructed, we found that the lateral root identities gradually weakened, whereas pluripotency identities were gradually induced and enriched in QC-like cells (Figure 4A–4D). These cell-fate transition characteristics offer new insights into the development of callus formation and also provide the possibility of exploring the mechanisms of cell fate determination, whereby LRPI-like cells

develop into callus and not a lateral root. For one thing, in addition to the expression of LRP cell marker genes and the stem cell marker gene *WOX5*, we also detected cuticle development, lipid transport, and VLCFA metabolism identities in LRPI-like cells. Certain lipid molecules have also been reported to participate in the transmission of cell signals that regulate cell proliferation and differentiation (DeBono et al., 2009; Lu et al., 2021), and VLCFAs are important signaling molecules that limit the acquisition of totipotency and the regeneration ability of pericycle cells (Shang et al., 2016; Ingram and Nawrath, 2017). Thus, the enrichment of genes encoding lipid transporters *LTP1* and *LTP2* in LRPI-like cells indicates that LRPI-like cells could have abundant lipid transport activities that regulate the growth of newborn cells and help regulate cell fate transitions during callus induction. For another, genes that gradually increase in expression during the development of LRPI-like cells into QC-like cells, such as those expressed in module 3, are likely to be potential determinant regulators. These are enriched in terms such as “response to cyclopentenone” and “snoRNA3’ end processing,” which have been reported to participate in cell differentiation (Barneche et al., 2000; Stintzi et al., 2001; Zhou et al., 2019; Ikeuchi et al., 2020). Cyclopentenone can act as an intermediate or signaling molecule for JA to activate or inhibit the JA signaling pathway, and JA signaling can inhibit cell differentiation and place cells in a less differentiated state (Stintzi et al., 2001; Zhou et al., 2019; Ikeuchi et al., 2020). In addition, TFs and target genes are involved in the unique TFRN responsible for activating the regenerative activity of QC-like cells. These include *TCP23*, *GFB4*, *RTV1*, and *bHLH104*, whose target genes facilitate the performance of QC-like functions such as auxin transport, cell proliferation and differentiation, and meristem initiation. Investigation of the key cross-regulators involved in turning off expression of lateral root developmental genes and turning on expression of callus identity genes would also be worthwhile. These genes may provide a reference gene pool for further functional regulatory exploration to improve the efficiency of callus induction.

Relative to animals, plants have unparalleled multi-scale regenerative potential, ranging from the regeneration of specific cell types, tissues, and organs, to the rebuilding of an entire organism. However, the question of whether the mechanism of callus induction is conserved across species has not been satisfactorily addressed. In this study, we performed a comparative analysis of callus formation within and across species. Comparison of *Arabidopsis* root callus and hypocotyl callus showed that there is a strong correlation between callus cells derived from different explants, and the QC-like cells in our dataset showed a significant correlation with EV & CF cells in a previously reported dataset for hypocotyl-derived callus. They were also found to share a series of regulators involved in callus induction, even across different sample time points. We also carried out a comparative analysis of callus induction between *Arabidopsis* and cotton. We found that genes specifically expressed in the primary vascular cells of cotton, which are the main cell type for callus initiation, were generally enriched in *Arabidopsis* CIM1 cells, and the largest proportion of these genes were co-expressed with *Arabidopsis* XPP cells. This result provides new evidence for a conserved callus formation mechanism from a novel perspective. However, to explore the possible reasons why the efficiency of callus induction varies substantially among tissues

and species, chromatin accessibility analysis at the single-cell level should be performed.

In summary, we identified heterogeneity among cells and cell-type composition during callus induction. However, the degree to which these cell types are organized with each other to regulate the formation of pluripotent callus cells is also an important and interesting question that has not yet been fully answered. In future work, spatial transcriptome studies would not only provide a more detailed spatiotemporal cell-type atlas for callus induction (Xia et al., 2022; Yin et al., 2023) but would also facilitate a better understanding of cell sociality and the mechanisms that regulate callus induction.

METHODS

Plant growth conditions and induction of callus formation

Arabidopsis thaliana Col-0 was used as the wild type. Seeds were surface sterilized with 8% sodium hypochlorite and 0.1% Triton X-100 solution and then grown on 1/2 Murashige and Skoog (MS) medium (Sigma M5519) at 25°C under 16-h light/8-h dark conditions. Root explants were cut from 5-day-old seedlings and cultured in CIM (MS medium, 3% w/v sucrose, 0.3% w/v Phytagel, 0.22 µM N-(phenylmethyl)-9H-purin-6-amine, and 4.52 µM 2,4-dichlorophenoxyacetic acid, pH 5.7) under 24-h dark conditions at 25°C for callus induction.

scRNA-seq

Root explants were cultured in CIM, and samples were collected on days 0, 1, and 4. All calli were digested in protoplast isolation solution containing 1% w/v cellulase “Onozuka” R-10 (Yakult Pharmaceutical), 0.2% w/v macerozyme R-10 (Yakult Pharmaceutical), 0.1% w/v pectinase (Sigma, 17389), 20 mM MES (pH 5.7, Sigma, M3671), 10 mM CaCl₂ (Sigma, C5670), 10 mM KCl (Sigma, P5405), 0.4 M D-mannitol (Sigma, M1902), and 0.1% BSA (Sigma, V900933) for approximately 2 h on a shaker at 60 rpm in the dark. To remove the enzyme solution and tissue debris, the digested tissue suspensions were filtered through 40-µm nylon mesh and washed with W5 buffer, including 154 mM NaCl (Sigma, S5886), 5 mM KCl (Sigma, P5405), 125 mM CaCl₂, and 2 mM MES (pH 5.7). The mixed solutions were gently centrifuged at 100 g for 5 min to collect protoplasts, which were washed, resuspended in W5 buffer at a concentration of 2 × 10⁶ cells/mL, and counted using a hemocytometer.

Single-cell RNA-seq was performed using a DNBelab C4 system. The CIM0 root explants produced three replicates, and the CIM1 and CIM4 root explants produced two replicates. All libraries were prepared using the BGISEQ-T1 sequencing platform. DNA nanoballs were loaded into the patterned nanoarrays and sequenced with a BGISEQ-T1 sequencer with the following read lengths: 41 bp for read 1, 100 bp for read 2, and 10 bp for the sample index.

Processing of scRNA-seq data

Single-cell RNA-seq data were mapped to the TAIR10 *Arabidopsis* genome using STAR. The level of gene expression in each cell was calculated using unique molecular identifiers (UMIs) with PISA (<https://github.com/pisa-engine/pisa>).

Data filtering, dimension reduction, cell clustering, and DEG identification were performed using Seurat 3.0. First, cells with fewer than 100 genes, more than 5000 genes, or more than 10% mitochondrial genes were filtered out. According to the expression of G2/M and S phase markers (Supplemental Table 1), the cell-cycle stage was computed for each cell using the Seurat function CellCycleScoring. After running the CellCycleScoring function, SCTransform was performed again to regress out the cell-cycle effects by defining vars.to.regress augmented with S.Score and G2M.Score. In subsequent dimensional reduction, scaled

Plant Communications

residuals of the remaining genes were used, which avoided clustering cells in relation to their cell-cycle stages, reads, and mitochondrial genes. Genes induced by protoplasting were also removed (Birnbaum et al., 2003). Finally, the matrix of three CIM0 replicates, two CIM1 replicates, and two CIM4 replicates contained 6184, 8777, and 10 227 cells for downstream analysis, respectively.

Cell clustering

The function “SCTransform” was used to normalize, scale, and transform the data. Next, the “RunPCA” function was used to reduce linear dimensionality, and the “FindNeighbors” and “FindClusters” functions were used for cell clustering using the top 30 PCs and a 0.8 resolution.

DEG analysis

Drawing on the Wilcoxon rank-sum test included in the Seurat package, the differential expression of cell types or cell subtypes was determined by comparing the mean transcript levels of cells in a given cluster with those in all other clusters. Two criteria were used: logfc.threshold = 0.2 and min.pct = 0.25.

Identification of cell types

Cell types were annotated using root cell-type marker genes (Brady et al., 2007; Efroni et al., 2016; Denyer et al., 2019; Jean-Baptiste et al., 2019; Ryu et al., 2019; Serrano-Ron et al., 2021; Zhai and Xu, 2021). Because callus cells are in a mixed cell state, it is not sufficient to use a few marker genes to distinguish one cell cluster from another; therefore, we also used the AUCell method to assist in the identification of cell types. This method uses the area under the curve to determine whether a key subset of genes in an input gene set is enriched in the expressed genes of an individual cell (Aibar et al., 2017). Annotations of the marker genes are given in *Supplemental Table 2*.

Correlation analysis

The R function “cor” was used to perform correlation analysis for the whole transcriptome of each single-cell sample. The distance used was Euclidian, and the “kendall” cluster method was used for normalized data for each sample calculated by Seurat.

Trajectory analysis

We used the R package Monocle 3 (v1.3.10) to construct a global developmental trajectory for callus formation. To begin, we converted Seurat objects into monocle 3 “cell_data_set” objects using “new_cell_data_set” functions. The monocle 3 object was then standardized, reduced, and clustered using the functions “Preprocess_cds,” “reduce_dimension,” and “cluster_cells.” The coordinates in the monocle 3 object were replaced by the coordinates in the Seurat object with the “Embeddings” function, and trajectory inference was performed using the “Learn-graph” function. Finally, the cell developmental trajectory was visualized using the “plot_cells” function.

Pseudo-time analysis

Pseudo-time analysis was performed using the R packages Monocle 2 and CytoTRACE (Gulati et al., 2020). First, the function “newCellDataSet” was used to create a monocle 2 object. The number of genes expressed in each cell and the number of filtered genes expressed in fewer than 10 cells were then counted using the “detectGenes” function. The “dispersionTable” function was used to select genes with high dispersion between cells, and the top 2000 genes were chosen for trajectory construction. Finally, we calculated the frequency of pseudodifferentiation for each cell to infer its differentiation status using CytoTRACE.

Transcriptomic vector field inference

Transcriptomic vector field inference of RPI-like, VI-like, regenerative, and QC-like cells was performed using scTour (Li, 2023). Model training was performed using default parameters. We first used each type of cell in CIM-0D, CIM-1D, and CIM-4D to form the reference vector field. We in-

Cell-lineage transcriptome atlas for callus induction

ferred the latent representations of the top 1000 highly variable genes with both alpha_z and alpha_predz set to 0.5. To validate the intermediate position of CIM-4D RPI-like cells in the vector field, we excluded these cells and performed a prediction of the vector field for the remaining query cells. We inferred the latent representations of the top 1000 highly variable genes in the query cells with alpha_z set to 0.4, alpha_predz set to 0.6, and mode set to “coarse.” The “sct.vf.plot_vector_field” function was used to generate the vector field plots.

GO enrichment analyses

GO and KEGG enrichment analyses were performed using the clusterProfiler R package with the TAIR10 annotation as the background. We selected terms using $p < 0.05$ to indicate significantly enriched functions, with a smaller p value indicating more significant enrichment.

Calculation of gene set score

We used the “ssGSEA” function in the R package GSVA to calculate the score for a specific gene set in the single-cell matrix. We selected DEGs for LRP1-like cells and QC-like cells as specific gene sets and used the ssGSEA function to calculate the enrichment scores for these two types of gene sets in the LRP and hypocotyl single-cell gene matrices. The specific parameters set were method = “ssgsea” and kcdf = “Gaussian.”

TFRN analysis

We used pySCENIC 0.12.1 (Van de Sande et al., 2020) to identify the TFs that were responsible for triggering genes related to callus regeneration in cells of cluster 19. The TF list for co-expression construction and cisTarget databases for *Arabidopsis* were drawn from scPlant (Cao et al., 2023). By overlapping the TF lists from scPlant and PlantTFDB (Jin et al., 2016), we identified a consensus set of 674 *Arabidopsis* TFs for further analysis. The co-expression network between TFs and their potential target genes was derived from the raw count matrix using the “pyscenic grn” function. This primary network was subsequently refined, retaining only direct target genes that possessed corresponding binding motifs for the regulating TF in the “pyscenic ctx” step. A regulon consists of a specific TF and its direct target genes. The activity of the regulons was calculated and binarized using “pyscenic AUCell.” Finally, the selected network was visualized with Cytoscape 3.9.1.

DATA AND CODE AVAILABILITY

The sequencing data for *Arabidopsis thaliana* that support the findings of this study have been deposited in the China National GeneBank (CNGB) Sequence Archive (Guo et al., 2020) of the CNGB Database (Chen et al., 2020) with accession number CNP0004389. In addition, we generated a database for the *Arabidopsis* callus single-cell transcriptional atlas in STOmicsDB (Xu et al., 2024), and the clustering and gene expression results are given visual representation at <https://db.cngb.org/genebank/arabidopsis/singlecell>.

SUPPLEMENTAL INFORMATION

Supplemental information is available at *Plant Communications Online*.

FUNDING

This research was supported by the National Key R&D Program of China (2022YFC3400300), the Guangdong Provincial Key Laboratory of Genome Read and Write (no. 2017B030301011), the Shenzhen Key Laboratory of Single-Cell Omics (no. ZDSYS20190902093613831), the Guangdong Genomics Data Center (2021B121210001), and the theme project of Shenzhen Institute of Synthetic Biology (no. ZTXM20190004).

AUTHOR CONTRIBUTIONS

Conceptualization, X.X. and K.K.X.; methodology, R.L.Y. and R.Y.C.; formal analysis, R.L.Y. and R.Y.C.; investigation, R.L.Y.; data curation,

R.L.Y.; writing – original draft, R.L.Y. and K.K.X.; writing – review & editing, R.L.Y. and K.K.X.; supervision, X.X. and K.K.X.

ACKNOWLEDGMENTS

We are sincerely thankful for the support provided by the China National GeneBank (CNGB) and for the help of Dr. Jiming Li and Tao Yang. No conflict of interest is declared.

Received: November 18, 2023

Revised: April 16, 2024

Accepted: May 6, 2024

Published: May 7, 2024

REFERENCES

- Aibar, S., González-Blas, C.B., Moerman, T., Huynh-Thu, V.A., Imrichova, H., Hulselmans, G., Rambow, F., Marine, J.-C., Geurts, P., Aerts, J., et al. (2017). SCENIC: single-cell regulatory network inference and clustering. *Nat. Methods* **14**:1083–1086.
- Aida, M., Beis, D., Heidstra, R., Willemsen, V., Blilou, I., Galinha, C., Nussaume, L., Noh, Y.-S., Amasino, R., and Scheres, B. (2004). The *PLETHORA* genes mediate patterning of the *Arabidopsis* root stem cell niche. *Cell* **119**:109–120.
- Albini, S., Zakharova, V., and Ait-Si-Ali, S. (2019). Histone modifications. In *Epigenetics and Regeneration* (Academic Press), pp. 47–72.
- Atta, R., Laurens, L., Boucheron-Dubuisson, E., Guivarc'h, A., Carnero, E., Giraudat-Pautot, V., Rech, P., and Chiriqui, D. (2009). Pluripotency of *Arabidopsis* xylem pericycle underlies shoot regeneration from root and hypocotyl explants grown in vitro. *Plant J.* **57**:626–644.
- Barneche, F., Steinmetz, F., and Echeverría, M. (2000). Fibrillarin Genes Encode Both a Conserved Nucleolar Protein and a Novel Small Nucleolar RNA Involved in Ribosomal RNA Methylation in *Arabidopsis thaliana*. *J. Biol. Chem.* **275**:27212–27220.
- Birnbaum, K., Shasha, D.E., Wang, J.Y., Jung, J.W., Lambert, G.M., Galbraith, D.W., and Benfey, P.N. (2003). A gene expression map of the *Arabidopsis* root. *Science* **302**:1956–1960.
- Brady, S.M., Orlando, D.A., Lee, J.-Y., Wang, J.Y., Koch, J., Dinneny, J.R., Mace, D., Ohler, U., and Benfey, P.N. (2007). A high-resolution root spatiotemporal map reveals dominant expression patterns. *Science* **318**:801–806.
- Cao, S., He, Z., Chen, R., Luo, Y., Fu, L.-Y., Zhou, X., He, C., Yan, W., Zhang, C.-Y., and Chen, D. (2023). scPlant: a versatile framework for single-cell transcriptomic data analysis in plants. *Plant Commun.* **4**, 100631.
- Chen, F.Z., You, L.J., Yang, F., Wang, L.N., Guo, X.Q., Gao, F., Hua, C., Tan, C., Fang, L., Shan, R.Q., et al. (2020). CNGBdb: China National GeneBank DataBase. *Yi chuan=Hereditas* **42**:799–809.
- Chen, L., Tong, J., Xiao, L., Ruan, Y., Liu, J., Zeng, M., Huang, H., Wang, J.-W., and Xu, L. (2016). *YUCCA*-mediated auxin biogenesis is required for cell fate transition occurring during de novo root organogenesis in *Arabidopsis*. *J. Exp. Bot.* **67**:4273–4284.
- DeBono, A., Yeats, T.H., Rose, J.K.C., Bird, D., Jetter, R., Kunst, L., and Samuels, L. (2009). *Arabidopsis LTPG* is a glycosylphosphatidylinositol-anchored lipid transfer protein required for export of lipids to the plant surface. *Plant Cell* **21**:1230–1238.
- Denyer, T., Ma, X., Klesen, S., Scacchi, E., Nieselt, K., and Timmermans, M.C.P. (2019). Spatiotemporal developmental trajectories in the *Arabidopsis* root revealed using high-throughput single-cell RNA sequencing. *Dev. Cell* **48**:840–852.e5.
- Efroni, I., Mello, A., Nawy, T., Ip, P.-L., Rahni, R., DelRose, N., Powers, A., Satija, R., and Birnbaum, K.D. (2016). Root regeneration triggers an embryo-like sequence guided by hormonal interactions. *Cell* **165**:1721–1733.
- Eshed Williams, L. (2021). Genetics of shoot meristem and shoot regeneration. *Annu. Rev. Genet.* **55**:661–681.
- Fan, M., Xu, C., Xu, K., and Hu, Y. (2012). *LATERAL ORGAN BOUNDARIES DOMAIN* transcription factors direct callus formation in *Arabidopsis* regeneration. *Cell Res.* **22**:1169–1180.
- Fernandez, A.I., Vangheluwe, N., Xu, K., Jourquin, J., Claus, L.A.N., Morales-Herrera, S., Parizot, B., De Gernier, H., Yu, Q., Drozdzecki, A., et al. (2020). *GOLVEN* peptide signalling through *RGL* receptors and *MPK6* restricts asymmetric cell division during lateral root initiation. *Nat. Plants* **6**:533–543.
- Forzani, C., Aichinger, E., Sornay, E., Willemsen, V., Laux, T., Dewitte, W., and Murray, J.A.H. (2014). *WOX5* suppresses *CYCLIN D* activity to establish quiescence at the center of the root stem cell niche. *Curr. Biol.* **24**:1939–1944.
- Gulati, G.S., Sikandar, S.S., Wesche, D.J., Manjunath, A., Bharadwaj, A., Berger, M.J., Ilagan, F., Kuo, A.H., Hsieh, R.W., Cai, S., et al. (2020). Single-cell transcriptional diversity is a hallmark of developmental potential. *Science* **367**:405–411.
- Guo, X., Chen, F., Gao, F., Li, L., Liu, K., You, L., Hua, C., Yang, F., Liu, W., Peng, C., et al. (2020). CNSA: a data repository for archiving omics data. *Database* **2020**, baaa055.
- Hofhuis, H., Laskowski, M., Du, Y., Prasad, K., Grigg, S., Pinon, V., and Scheres, B. (2013). Phyllotaxis and rhizotaxis in *Arabidopsis* are modified by three *PLETHORA* transcription factors. *Curr. Biol.* **23**:956–962.
- Hu, X., and Xu, L. (2016). Transcription factors *WOX11/12* directly activate *WOX5/7* to promote root primordia initiation and organogenesis. *Plant Physiol.* **172**:2363–2373.
- Ikeuchi, M., Sugimoto, K., and Iwase, A. (2013). Plant callus: mechanisms of induction and repression. *Plant Cell* **25**:3159–3173.
- Ikeuchi, M., Rymen, B., and Sugimoto, K. (2020). How do plants transduce wound signals to induce tissue repair and organ regeneration? *Curr. Opin. Plant Biol.* **57**:72–77.
- Ikeuchi, M., Favero, D.S., Sakamoto, Y., Iwase, A., Coleman, D., Rymen, B., and Sugimoto, K. (2019). Molecular mechanisms of plant regeneration. *Annu. Rev. Plant Biol.* **70**:377–406.
- Ikeuchi, M., Iwase, A., Rymen, B., Lambolez, A., Kojima, M., Takebayashi, Y., Heyman, J., Watanabe, S., Seo, M., De Veylder, L., et al. (2017). Wounding triggers callus formation via dynamic hormonal and transcriptional changes. *Plant Physiol.* **175**:1158–1174.
- Ikeuchi, M., Iwase, A., Ito, T., Tanaka, H., Favero, D.S., Kawamura, A., Sakamoto, S., Wakazaki, M., Tameshige, T., Fujii, H., et al. (2022). Wound-inducible *WUSCHEL-RELATED HOMEBOX* 13 is required for callus growth and organ reconnection. *Plant Physiol.* **188**:425–441.
- Ingram, G., and Nawrath, C. (2017). The roles of the cuticle in plant development: organ adhesions and beyond. *J. Exp. Bot.* **68**:5307–5321.
- Ishiguro, S., Watanabe, Y., Ito, N., Nonaka, H., Takeda, N., Sakai, T., Kanaya, H., and Okada, K. (2002). SHEPHERD is the *Arabidopsis* *GRP94* responsible for the formation of functional CLAVATA proteins. *EMBO J.* **21**:898–908.
- Iwase, A., Harashima, H., Ikeuchi, M., Rymen, B., Ohnuma, M., Komaki, S., Morohashi, K., Kurata, T., Nakata, M., Ohme-Takagi, M., et al. (2017). *WIND1* promotes shoot regeneration through transcriptional activation of *ENHANCER OF SHOOT REGENERATION1* in *Arabidopsis*. *Plant Cell* **29**:54–69.
- Jean-Baptiste, K., McFainé-Figueroa, J.L., Alexandre, C.M., Dorrrity, M.W., Saunders, L., Bubb, K.L., Trapnell, C., Fields, S., Queitsch, C., and Cuperus, J.T. (2019). Dynamics of gene expression in single root cells of *Arabidopsis thaliana*. *Plant Cell* **31**:993–1011.

Plant Communications

- Jin, J., Tian, F., Yang, D.-C., Meng, Y.-Q., Kong, L., Luo, J., and Gao, G. (2016). PlantTFDB 4.0: toward a central hub for transcription factors and regulatory interactions in plants. *Nucleic Acids Res.* gkw982.
- Kareem, A., Durgaprasad, K., Sugimoto, K., Du, Y., Pulianmackal, A.J., Trivedi, Z.B., Abhayadev, P.V., Pinon, V., Meyerowitz, E.M., Scheres, B., et al. (2015). *PLETHORA* genes control regeneration by a two-step mechanism. *Curr. Biol.* **25**:1017–1030.
- Kim, J.Y., Yang, W., Forner, J., Lohmann, J.U., Noh, B., and Noh, Y.S. (2018). Epigenetic reprogramming by histone acetyltransferase HAG1/ATGCN5 is required for pluripotency acquisition in *Arabidopsis*. *EMBO J.* **37**, e98726.
- Li, Q. (2023). scTour: a deep learning architecture for robust inference and accurate prediction of cellular dynamics. *Genome Biol.* **24**:149.
- Liu, H., Zhang, H., Dong, Y.X., Hao, Y.J., and Zhang, X.S. (2018a). *DNA METHYLTRANSFERASE* 1-mediated shoot regeneration is regulated by cytokinin-induced cell cycle in *Arabidopsis*. *New Phytol.* **217**:219–232.
- Liu, J., Hu, X., Qin, P., Prasad, K., Hu, Y., and Xu, L. (2018b). The *WOX11-LBD16* pathway promotes pluripotency acquisition in callus cells during de novo shoot regeneration in tissue culture. *Plant Cell Physiol.* **59**:734–743.
- Liu, J., Sheng, L., Xu, Y., Li, J., Yang, Z., Huang, H., and Xu, L. (2014). *WOX11* and *12* are involved in the first-step cell fate transition during de novo root organogenesis in *Arabidopsis*. *Plant Cell* **26**:1081–1093.
- Lu, R., Zhang, J., Wu, Y.-W., Wang, Y., Zhang, J., Zheng, Y., Li, Y., and Li, X.-B. (2021). *bHLH* transcription factors *LP1* and *LP2* regulate longitudinal cell elongation. *Plant Physiol.* **187**:2577–2591.
- Matsuzaki, Y., Ogawa-Ohnishi, M., Mori, A., and Matsubayashi, Y. (2010). Secreted peptide signals required for maintenance of root stem cell niche in *Arabidopsis*. *Science* **329**:1065–1067.
- Mo, Y., and Jiao, Y. (2022). Advances and applications of single-cell omics technologies in plant research. *Plant J.* **110**:1551–1563.
- Ogura, N., Sasagawa, Y., Ito, T., Tameshige, T., Kawai, S., Sano, M., Doll, Y., Iwase, A., Kawamura, A., Suzuki, T., et al. (2023). *WUSCHEL-RELATED HOMEOBOX* 13 suppresses de novo shoot regeneration via cell fate control of pluripotent callus. *Sci. Adv.* **9**, eadg6983.
- Okushima, Y., Fukaki, H., Onoda, M., Theologis, A., and Tasaka, M. (2007). *ARF7* and *ARF19* regulate lateral root formation via direct activation of *LBD/ASL* genes in *Arabidopsis*. *Plant Cell* **19**:118–130.
- Pernas, M., Ryan, E., and Dolan, L. (2010). *SCHIZORIZA* controls tissue system complexity in plants. *Curr. Biol.* **20**:818–823.
- Pitaksaringkarn, W., Matsuoka, K., Asahina, M., Miura, K., Sage-Ono, K., Ono, M., Yokoyama, R., Nishitani, K., Ishii, T., Iwai, H., et al. (2014). *XTH 20* and *XTH 19* regulated by *ANAC 071* under auxin flow are involved in cell proliferation in incised *Arabidopsis* inflorescence stems. *Plant J.* **80**:604–614.
- Ryu, K.H., Huang, L., Kang, H.M., and Schiefelbein, J. (2019). Single-cell RNA sequencing resolves molecular relationships among individual plant cells. *Plant Physiol.* **179**:1444–1456.
- Serrano-Ron, L., Perez-Garcia, P., Sanchez-Corriñero, A., Gude, I., Cabrera, J., Ip, P.-L., Birnbaum, K.D., and Moreno-Risueno, M.A. (2021). Reconstruction of lateral root formation through single-cell RNA sequencing reveals order of tissue initiation. *Mol. Plant* **14**:1362–1378.
- Cell-lineage transcriptome atlas for callus induction
- Shahan, R., Nolan, T.M., and Benfey, P.N. (2021). Single-cell analysis of cell identity in the *Arabidopsis* root apical meristem: insights and opportunities. *J. Exp. Bot.* **72**:6679–6686.
- Shang, B., Xu, C., Zhang, X., Cao, H., Xin, W., and Hu, Y. (2016). Very-long-chain fatty acids restrict regeneration capacity by confining pericycle competence for callus formation in *Arabidopsis*. *Proc. Natl. Acad. Sci. USA* **113**:5101–5106.
- Shaw, R., Tian, X., and Xu, J. (2021). Single-cell transcriptome analysis in plants: advances and challenges. *Mol. Plant* **14**:115–126.
- Stintzi, A., Weber, H., Reymond, P., Browse, J., and Farmer, E.E. (2001). Plant defense in the absence of jasmonic acid: the role of cyclopentenones. *Proc. Natl. Acad. Sci. USA* **98**:12837–12842.
- Sugimoto, K., Jiao, Y., and Meyerowitz, E.M. (2010). *Arabidopsis* regeneration from multiple tissues occurs via a root development pathway. *Dev. Cell* **18**:463–471.
- Valvekens, D., Van Montagu, M., and Van Lijsebettens, M. (1988). Agrobacterium tumefaciens-mediated transformation of *Arabidopsis thaliana* root explants by using kanamycin selection. *Proc. Natl. Acad. Sci. USA* **85**:5536–5540.
- Van de Sande, B., Flerin, C., Davie, K., De Waegeneer, M., Hulselmans, G., Aibar, S., Seurinck, R., Saelens, W., Cannoodt, R., Rouchon, Q., et al. (2020). A scalable SCENIC workflow for single-cell gene regulatory network analysis. *Nat. Protoc.* **15**:2247–2276.
- Xia, K., Sun, H.-X., Li, J., Li, J., Zhao, Y., Chen, L., Qin, C., Chen, R., Chen, Z., Liu, G., et al. (2022). The single-cell stereo-seq reveals region-specific cell subtypes and transcriptome profiling in *Arabidopsis* leaves. *Dev. Cell* **57**:1299–1310.e4.
- Xu, C., Cao, H., Zhang, Q., Wang, H., Xin, W., Xu, E., Zhang, S., Yu, R., Yu, D., and Hu, Y. (2018). Control of auxin-induced callus formation by *bZIP59-LBD* complex in *Arabidopsis* regeneration. *Nat. Plants* **4**:108–115.
- Xu, Z., Wang, W., Yang, T., Li, L., Ma, X., Chen, J., Wang, J., Huang, Y., Gould, J., Lu, H., et al. (2024). STOMicsDB: a comprehensive database for spatial transcriptomics data sharing, analysis and visualization. *Nucleic Acids Res.* **52**:D1053–D1061.
- Yin, R., Xia, K., and Xu, X. (2023). Spatial transcriptomics drives a new era in plant research. *Plant J.* **116**:1571–1581.
- Zhai, N., and Xu, L. (2021). Pluripotency acquisition in the middle cell layer of callus is required for organ regeneration. *Nat. Plants* **7**:1453–1460.
- Zhang, J., Xia, K., Yang, Y., and Yang, H. (2015). Overexpression of *Arabidopsis* phosphoinositide-specific phospholipase C5 induces leaf senescence. *Plant Cell Tissue Organ Cult.* **120**:585–595.
- Zhang, T.-Q., Lian, H., Zhou, C.-M., Xu, L., Jiao, Y., and Wang, J.-W. (2017). A two-step model for de novo activation of *WUSCHEL* during plant shoot regeneration. *Plant Cell* **29**:1073–1087.
- Zhou, W., Lozano-Torres, J.L., Biliou, I., Zhang, X., Zhai, Q., Smart, G., Li, C., and Scheres, B. (2019). A jasmonate signaling network activates root stem cells and promotes regeneration. *Cell* **177**:942–956.e14.
- Zhu, X., Xu, Z., Wang, G., Cong, Y., Yu, L., Jia, R., Qin, Y., Zhang, G., Li, B., Yuan, D., et al. (2023). Single-cell resolution analysis reveals the preparation for reprogramming the fate of stem cell niche in cotton lateral meristem. *Genome Biol.* **24**:194.